A WAVEGUIDE MODEL FOR THE EVENING TYPE TRANSEQUATORIAL VHF PROPAGATION: COMPARISON WITH EXPERIMENT FOR THE EURO-AFRICAN SECTOR

Nikolaos K. Uzunoglu and Costas Fimerelis,
Department of Electrical Engineering, National Technical University of Athens, 106 82 Athens, Greece

ABSTRACT

A waveguide model is proposed for the evening type transequatorial propagation mode. Field aligned irregularities observed in equatorial ionosphere are assumed to form dielectric waveguides. A local Champan type layer electron density distribution is taken inside the guide. The transequatorial wave propagation is treated by using this model and the propagation theory of dielectric waveguides. The total attenuation is computed between two points located in opposite hemispheres. The analytic form of the results permits easy interpretation of the propagation characteristics. A good agreement is observed between the experimental results and the theoretical calculations for the total attenuation. Comparisons have also been done for the propagation delay and the incoming elevation angle at the reception point.

1. INTRODUCTION

Evening type Transequatorial Propagation (E-TEP) is a special propagation mode occuring mainly between magnetically conjugate points. It has well distinguishable characteristics from the Afternoon type Transequatorial Propagation (A-TEP) phenomena occuring on the same south-north hemisphere circuits. The main difference between these two propagation modes is that E-TEP takes place in exceedingly higher frequencies. As indicated from their naming, E-TEP and A-TEP occur in different daily hours. Fur-

Electromagnetics 8:1-13, 1988

thermore they have entirely different behavior as already discussed in detail by Nielson[1] and Cracknell et al.[2].

Several theoretical models have been proposed in the past to describe the propagation mechanism in TEP circuits. Initially a double refraction scheme from the ionospheric crests have been proposed[3]. Although this model explains quite satisfactorily the A-TEP phenomena, fails to predict the E-TEP basic characteristics[1]. Based on measurements of elevation angles and group delays on a circuit between Okinawa (Japan) and Darwin (Australia) a waveguide model has been suggested for the E-TEP[4]. The guiding of high frequency waves through field aligned irregularities has been examined theoretically by Nielson[5] and this theory has been extended by using numerical techniques to explain TEP phenomena by Heron et al.[6] Recently a whispering gallery mode has also been considered to describe TEP[7]. In the meantime the data gathered for the fine structure of ionosphere has shown that there are elongated irregularities aligned with the geomagnetic field lines in the equatorial ionosphere[8]. These are tubular shape depletion regions inside the equatorial ionosphere extending on both sides of magnetic equator at least from 5^{o} to 10^{o} (magnetic dip).

In this paper a dielectric waveguide model is proposed and is employed to analyse the E-TEP characteristics. In this analysis the propagation theory of dielectric waveguides is used extensively. Closed form analytical results are derived for the transmitted field strength. The numerical results obtained by applying this theory are compared with experimental results to verify the proposed theoretical model.

In fig. 1a the geometry of the proposed ionospheric duct is given. In the same figure a characteristic electron density distribution profile is also shown (Fig. 1b). Because of the Very High Frequencies (VHF) interested in this paper the electromagnetic characteristics of the ionosphere can be described with a scalar dielectric constant $\varepsilon = n^2$, where n is the corresponding refractive index. It is well known that,

$$n^2 = 1 - \frac{81N(cm^{-3})}{f^2(kHz)} \tag{1}$$

where $N(cm^{-3})$ is the electron density and f(kHz) is the radiation frequency.

The ionospheric duct is taken of circular cross section and its axis is assumed to be parallel to the magnetic field lines as illustrated in fig. 1a. In order to describe the propagation through the ionospheric duct the conventional polar cylindrical coordinates ρ,φ,z are introduced. In treating the waveguiding inside the ionospheric duct the curvature of the propagation axis is neglected and is taken to be a straight line. A widely used established theoretical model for the electron density profiles in ionosphere is the Chapman distribution[9]. In this paper also a similar distribution is adopted. According to the observations given in ref. 8 the electron density distribution inside the duct region is taken to be,

$$N(\rho) = N(o)(1-(\frac{\rho}{a})^2) \tag{2}$$

where $\rho=a$ is an equivalent radius of the irregularity region. Of course eq. (2) is valid only in the vicinity of the ionospheric duct and for $\rho>>a$ the conventional electron density profiles holds.

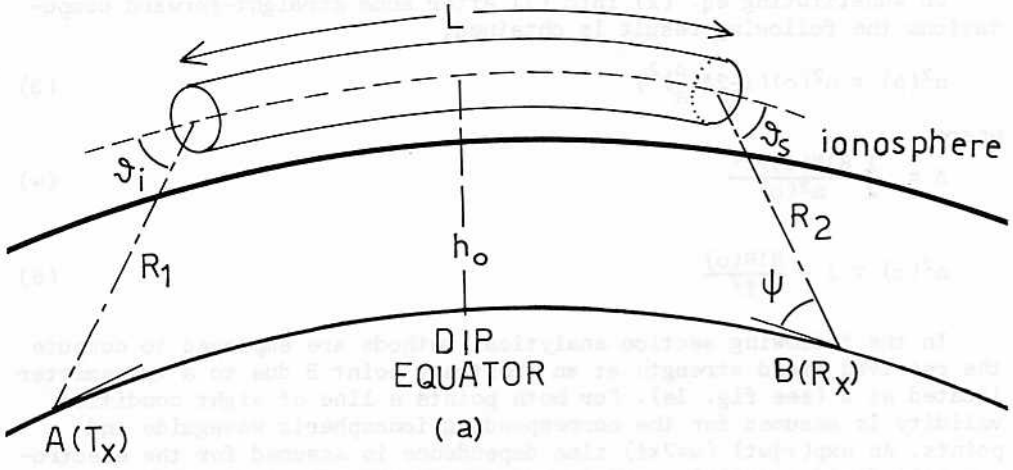

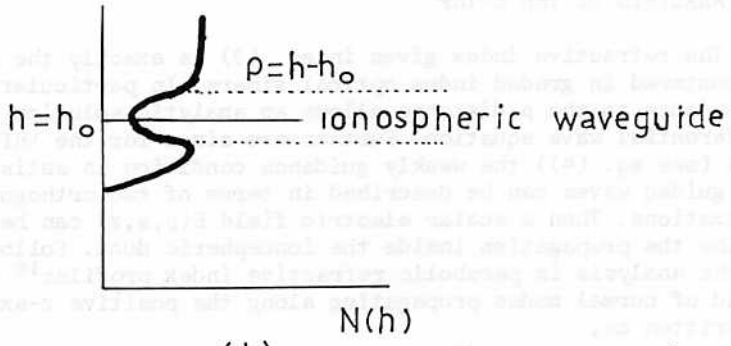

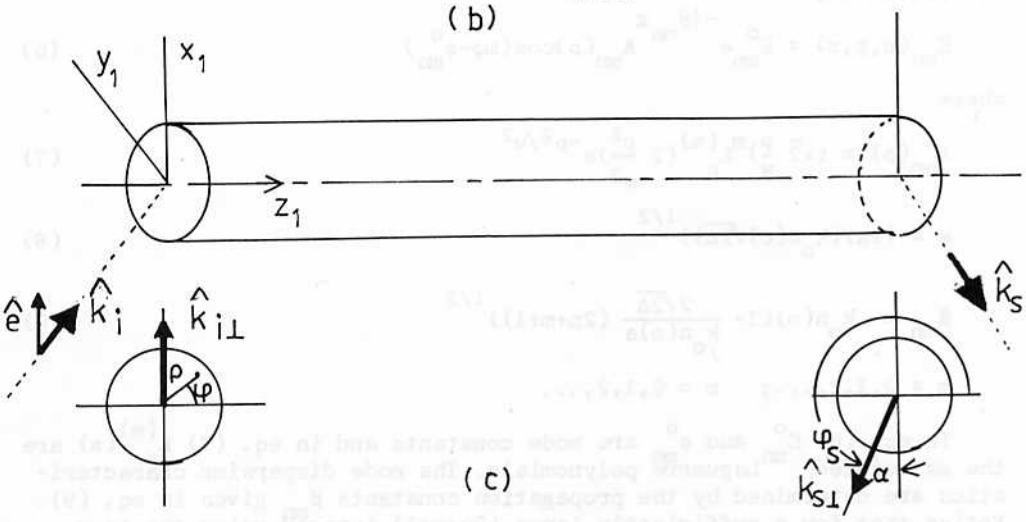

Fig. 1 (a) Propagation geometry
(b) Characteristic electron density
(c) Duct model geometry

On substituting eq. (2) into (1) after some straight-forward computations the following result is obtained,

$$n^2(\rho) = n^2(o)(1-2\Delta(\frac{\rho}{a})^2) \tag{3}$$

where

$$\Delta = \frac{1}{2}\frac{81N(o)/f^2}{n^2(o)} \tag{4}$$

$$n^2(o) = 1 - \frac{81N(o)}{f^2} \tag{5}$$

In the following section analytical methods are employed to compute the received field strength at an arbitrary point B due to a transmitter located at A (see fig. 1a). For both points a line of sight condition validity is assumed for the corresponding ionospheric waveguide end points. An $\exp(+j\omega t)$ ($\omega=2\pi f$) time dependence is assumed for the electromagnetic field quantities and is suppressed throughout the analysis.

2. ANALYSIS OF THE E-TEP

The refractive index given in eq. (3) is exactly the same with those encountered in graded index optical fibers. In particular the parabolic dependence to the ρ distance allows an analytic solution to the radial differential wave equation. Furthermore since for the VHF frequencies $\Delta<<1$ (see eq. (4)) the weakly guidance condition is satisfied. Therefore the guided waves can be described in terms of two orthogonal linear polarizations. Then a scalar electric field $E(\rho,\varphi,z)$ can be used to describe the propagation inside the ionospheric duct. Following the results of the analysis in parabolic refractive index profiles[10] the electric field of normal modes propagating along the positive z-axis (fig. 1c) can be written as,

$$E_{mn}(\rho,\varphi,z) = E^o_{mn} e^{-j\beta_{mn}z} A_{mn}(\rho)\cos(m\varphi-\varphi^o_{mn}) \tag{6}$$

where

$$A_{mn}(\rho) = (\sqrt{2}\frac{\rho}{w})^m L_n^{(m)}(2\frac{\rho^2}{w^2})e^{-\rho^2/w^2} \tag{7}$$

$$w = (2a/(k_o n(o)\sqrt{2\Delta}))^{1/2} \tag{8}$$

$$\beta_{mn} = k_o n(o)(1-\frac{2\sqrt{2\Delta}}{k_o n(o)a}(2n+m+1))^{1/2} \tag{9}$$

$m = 0,1,2,\ldots;\quad m = 0,1,2,\ldots$

In eq. (6) E^o_{mn} and φ^o_{mn} are mode constants and in eq. (7) $L_n^{(m)}(x)$ are the associated Laguerre polynomials. The mode dispersion characteristics are determined by the propagation constants β_{mn} given in eq. (9). Notice that for a sufficiently large (2n+m+1) integer value the term under the square root takes negative values and then β_{mn} is a purely imaginary quantity. In this case propagation doesn't take place.

Consider now the TEP propagation geometry of fig. 1a. Assume a linear-

ly polarized incident wave due to a transmitter located at the point A. A local coordinate system is defined at the entrance of the waveguide as shown in fig. 1c. The x_1 axis is taken inside the plane defined with the incident wave electric field polarization $\hat{e}$ and propagation direction defined with the unit vector $\hat{k}_i$ shown also in fig. 1c. The incident wave electric field on the waveguide input aperture can be written as

$$\underset{\sim}{E}_1 = \hat{e}\,\frac{\sqrt{60P_tG_t}}{R_1}\,e^{-jk_oR_1}\,e^{jk_o\hat{k}_i\cdot r_1} \tag{10}$$

where P_t is the emitted power,

G_t transmitter antenna gain,
R_1 distance between the point A and the input aperture center,
k_o free space propagation constant ($=2\pi/\lambda$, λ being the radiation wavelength),
$\underset{\sim}{\rho}_1$ position vector of an arbitrary point on the guide input aperture.

Introducing the expressions $\hat{k}_i = \hat{x}_1\sin\vartheta_i + \hat{z}_1\cos\vartheta_i$ and $\underset{\sim}{\rho}_1 = x_1\hat{x}_1 + y_1\hat{y}_1 = \rho_1\underset{\sim}{\rho}_1$ into eq. (10) with ϑ_i being the angle between the incident direction and z axis, the following result is obtained

$$\underset{\sim}{E}_1 = \hat{e}\,\frac{\sqrt{60P_tG_t}}{R_1}\,e^{-jk_oR_1}\,e^{jk_o\rho_1\cos\varphi_1\sin\vartheta_i} \tag{11}$$

where $x_1 = \rho_1\cos\varphi_1$, $\quad y_1 = \rho_1\sin\varphi_1$.

The electromagnetic field induced inside the ionospheric waveguide can be written in terms of a superposition of propagating normal modes given in eq. (6),

$$\underset{\sim}{E}_w(\rho_1,\varphi_1,z_1) = \hat{e}\sum_n\sum_m E^o_{nm}e^{-j\beta_{mn}z_1}A_{mn}(\rho_1)\cos(m\varphi_1) \tag{12}$$

Neglecting the diffraction phenomena, at the $z_1 = 0$ input aperture the following boundary conditions should be satisfied,

$$\underset{\sim}{E}_1\cdot\hat{x}_1 = \underset{\sim}{E}_w\cdot\hat{x}_1\Big|_{z_1=0} \tag{13}$$

where $\hat{x}_1$ is the unit vector along the x_1 axis.

Substituting eqs. (11),(12) into (13) and then multiplying both sides with the function

$$A_{m'n'}(\rho_1)\cos(m'\varphi_1)$$

and integrating on the input aperture by employing the orthogonality relations

$$\int_0^{2\pi} d\varphi_1\cos(m\varphi_1)\cos(m'\varphi_1) = \delta_{mm'}\frac{2\pi}{\varepsilon_m} \tag{14}$$

$$\int_0^{+\infty} dx\, e^{-x} x^m L_n^{(m)}(x) L_{n'}^{(m)}(x)dx = \delta_{nn'} \frac{(n+m)!}{n!} \tag{15}$$

where $\delta_{mm'}$ is the Kronecker symbol and

$$\epsilon_m = \begin{cases} 1 \text{ for } m=0 \\ 2 \text{ for } m\neq 0 \end{cases}$$

the following result is obtained

$$E_{nm}^{o} = \frac{\cos\vartheta_i \sqrt{60 P_t G_t}}{\frac{w^2}{2}\frac{(n+m)!}{n!}\frac{\pi}{\epsilon_m}} \int_0^{+\infty} \rho_1 d\rho_1 \int_0^{2\pi} d\varphi_1 \exp(jk_o\rho_1 \sin\vartheta_i \cos\varphi_1) \cdot$$

$$\cdot A_{mn}(\rho_1)\cos(m\varphi_1) \tag{16}$$

Introducing into eq. (16) the expansion[11]

$$\exp(jk_o\rho_1\sin\vartheta_i\cos\varphi_1) = \sum_{k=0}^{\infty} \epsilon_k j^k J_k(k_o\rho_1\sin\vartheta_i)\cos(k\varphi_1) \tag{17}$$

and by using the transformation[11]

$$\frac{(-1)^n}{2} \int_0^{+\infty} dy\, y^{m/2} L_n^{(m)}(y) e^{-y/2} J_m(\sqrt{xy}) = e^{-x/2} x^{m/2} L_n^{(m)}(x) \tag{18}$$

instead of eq. (16) we have,

$$E_{mn}^{o} = 2\cos\vartheta_i \frac{\sqrt{60 P_t G_t}}{R_1} e^{-jk_o R_1} j^m \epsilon_m e^{-x_i/2} x_i^{m/2} L_n^{(m)}(x_i) \cdot (-1)^n \frac{n!}{(m+n)!} \tag{19}$$

where

$$x_i = \frac{k_o w}{\sqrt{2}} \sin\vartheta_i \tag{20}$$

Substituting the mode coefficients into eq. (12) the guided wave field distribution can be computed at an arbitrary distance $z_1 = z$ along the guide axis. In particular by setting $z_1 = L$ equal to the guide length the field at the output aperture can be computed. Assuming again the reflection phenomena to be negligible the field on the $z_1=L$ output aperture can be taken equal to the incident wave $\underset{\sim}{E}_w(\rho_1,\varphi_1,L)$. In order to compute the field at the reception point B the following diffraction formula is employed[12],

$$\underset{\sim}{E}_r = jk_o\cos\vartheta_s \frac{e^{-jk_o R_2}}{2\pi R_2} \int_{\rho_1=0}^{\infty} \rho_1 d\rho_1 \int_{\varphi_1=0}^{2\pi} d\varphi_1 e^{jk_o \hat{k}_s \cdot \underset{\sim}{\rho}_1} \underset{\sim}{E}_w(\rho_1,\varphi_1,L) \tag{21}$$

where $\hat{k}_s$ is the unit vector along the line connecting the output aperture center and the reception point B. Defining the angles ϑ_s and φ_s as given in fig. 1c, the $\hat{k}_s$ unit vector can be written as

$$\hat{k}_s = \hat{z}_1\cos\vartheta_s + \sin\vartheta_s(\hat{x}_1\cos\varphi_s + \hat{y}_1\sin\varphi_s) \tag{22}$$

Substituting eq. (22) into (21) after a procedure similar to that given from eq. (14) to (19) the electric field vector at the reception point was found to be

$$\underset{\sim}{E}_r = \hat{e} jk_o \frac{w^2}{2} \frac{e^{-jk_o(R_1+R_2)}}{R_1R_2} \sqrt{60P_tG_t}\cos\vartheta_i\cos\vartheta_s \cdot e^{-\frac{(x_i+x_s)}{2}} S(\varphi_s,x_i,x_s) \tag{23}$$

where

$$x_s = \frac{k_o w}{\sqrt{2}} \sin\vartheta_s$$

$$S(\varphi_s,x_i,x_s) = \sum_n \sum_m (-1)^m \cos(m\varphi_s)\varepsilon_m e^{-j\beta_{mn}L} \cdot$$

$$\cdot \frac{n!}{(m+n)!} L_n^{(m)}(x_i) L_n^{(m)}(x_s)(x_i x_s)^{m/2} \tag{24}$$

As shown in the appendix the series given in eq. (24) can be summed approximately. Then the following result is obtained,

$$S(\varphi_s,x_i,x_s) = \frac{j}{2} \frac{e^{-jk_o n(o)L}}{\sin(\frac{\sqrt{2}\Delta L}{a})} \cdot \exp\{-\frac{j}{2}\cot(\frac{\sqrt{2}\Delta L}{a})(x_i+x_s+2\sqrt{x_i x_s}\cos\varphi_s)$$

$$+ \frac{1}{2}(x_i+x_s+2\sqrt{x_i x_s}\cos\varphi_s)\} \tag{25}$$

The refractive index n(o) up to now is assumed to be a purely real quantity. In order to take into account the imperfect structure of the ionospheric duct, which will cause scattering, the n(o) will be taken as a complex number with a small imaginary part, that is $n(o)=n'(o)-jn''(o)$ with $n''(o)<<n'(o)$. Furthemore the passing of the signal through the ionospheric layers before and after the waveguiding will result into Faraday rotation type depolarizations[2]. Because of the randomness of this effect, a $1/\sqrt{2}$ factor will be introduced in computing the $|E_r|$ field strength. Then using eqs. (23), (25) after some simple algebra the following result is obtained

$$|\underset{\sim}{E}_r| = \frac{k_o w^2}{4} \frac{\sqrt{30P_tG_t}}{R_1R_2} \cos\vartheta_i\cos\vartheta_s \frac{\exp(-\frac{k_o w}{\sqrt{2}}\sqrt{\sin\vartheta_i\sin\vartheta_s}\cos\alpha)}{\sin(\frac{\sqrt{2}\Delta L}{a})} \cdot \exp(-k_o n''(o)L) \tag{26}$$

where $\alpha = \pi-\varphi_s$. Notice that φ_s is the angle between the $\hat{x}$ axis and the projection of $\hat{k}_s$ into the transversal plane of the ionospheric guide as shown in fig. 1c. Because of the south-north transmission geometry always $\varphi_s \sim \pi$ and therefore $\alpha \sim 0$.

If the receiver antenna gain is G_r then the overall attenuation using eq. (26) is found to be

$$A = \frac{P_r}{P_t} = \frac{1}{32} \frac{G_rG_t}{R_1^2R_2^2} w^4(\cos\vartheta_i\cos\vartheta_s)^2 \exp(-2k_o n''_{(o)}L) \cdot$$

$$\cdot \frac{\exp(-\sqrt{2}\, k_o w \sqrt{\sin\vartheta_i \sin\vartheta_s}\cos\alpha)}{\sin^2(\frac{\sqrt{2}\Delta L}{a})} \qquad (27)$$

It is interesting to examine the contribution of each term into overall attenuation. The $(R_1R_2)^{-2}$ term represents the free space loss while the $(\cos\vartheta_i\cos\vartheta_s)^2$ is the polarization mismatch loss. The most important and interesting term is the $\exp(-\sqrt{2}\, k_o w\sqrt{\sin\vartheta_i\sin\vartheta_s}\cos\alpha)$. As already mentioned $\alpha=0$ and $k_o w$ by employing eqs. (8), (4), (5) found to be $k_o w = 3.05\, f(MHz)\sqrt{a}/\sqrt{N(o)}$. Introducting the numerical data f=144 MHz, a=25 Km and $N(o) = 10^5 cm^{-3}$ it is found that $k_o w \approx 3900$. Therefore in order to have minimum attenuation the terms $(\sin\vartheta_i\sin\vartheta_s)$ should be close to zero as much as possible. In case of a point illuminated directly from the waveguide axis it is possible to have $\vartheta_i=0$ or $\vartheta_s=0$. Minimum attenuation is achieved on radio links crossing perpendicular the magnetic equator provided that ϑ_i and ϑ_s are sufficiently small. Therefore, where the magnetic field is uniform over earth surface, the magnetic conjugency is the main condition to have a small attenuation. The $\exp(-2k_o n''(o)L)$ term represents the scattering losses inside the waveguide and has been introduced on a phenomenological ground. In the next section the possible values of $n''(o)$ will be discussed. Finally the term $\sin(\sqrt{2}\Delta L/a)$ appearing in the denominator arises from the superposition of normal mode field distributions at the waveguide output aperture. For specific frequencies it is possible to have $\sqrt{2}\Delta L/a = n\pi$ $(n=0,1,2,\ldots)$ and then $A \to +\infty$. From the analysis given in the appendix it is shown that this condition corresponds to the in phase superposition of all travelling modes. The non-physical result $A \to +\infty$ seems to arise because of the approximate β_{mn} propagation constants and the infinite number of modes used in summing up the series $S(\varphi_s, x_i, x_s)$ (see appendix). Since in practice the resonance condition $\sqrt{2}\Delta L/a = n\pi$ cannot be satisfied exactly, the $A \to \infty$ non physical result is not considered being a serious problem.

In computing the total propagation delay between the transmitter and receiver the summing of the delays occuring on the paths is considered.

$$\tau = \frac{R_1}{C} + \frac{R_2}{C} + \frac{L}{n(o)C} \qquad (28)$$

where $C = 3\times10^8$ m/s.

Note that the group velocity inside the ionospheric guide is taken approximately equal to $v_g = \partial\omega/\partial\beta_{m,n} \approx n(o)C$ for sufficiently small (2n+m+1) values (see eq.(9)).

3. COMPARISON WITH EXPERIMENTAL RESULTS

In this section numerical results obtained by applying the analytical expressions of sec. 2 will be compared with measurements done on Pretoria (South Africa) - Athens (Greece) and Harare (Zimbabwe)-Athens VHF circuits.

Details of the equipment characteristics used at transmission (Pretoria and Harare) and reception stations (Athens), measurement techniques and results as well, are described in detail elsewhere[2,13]. In fig. 2

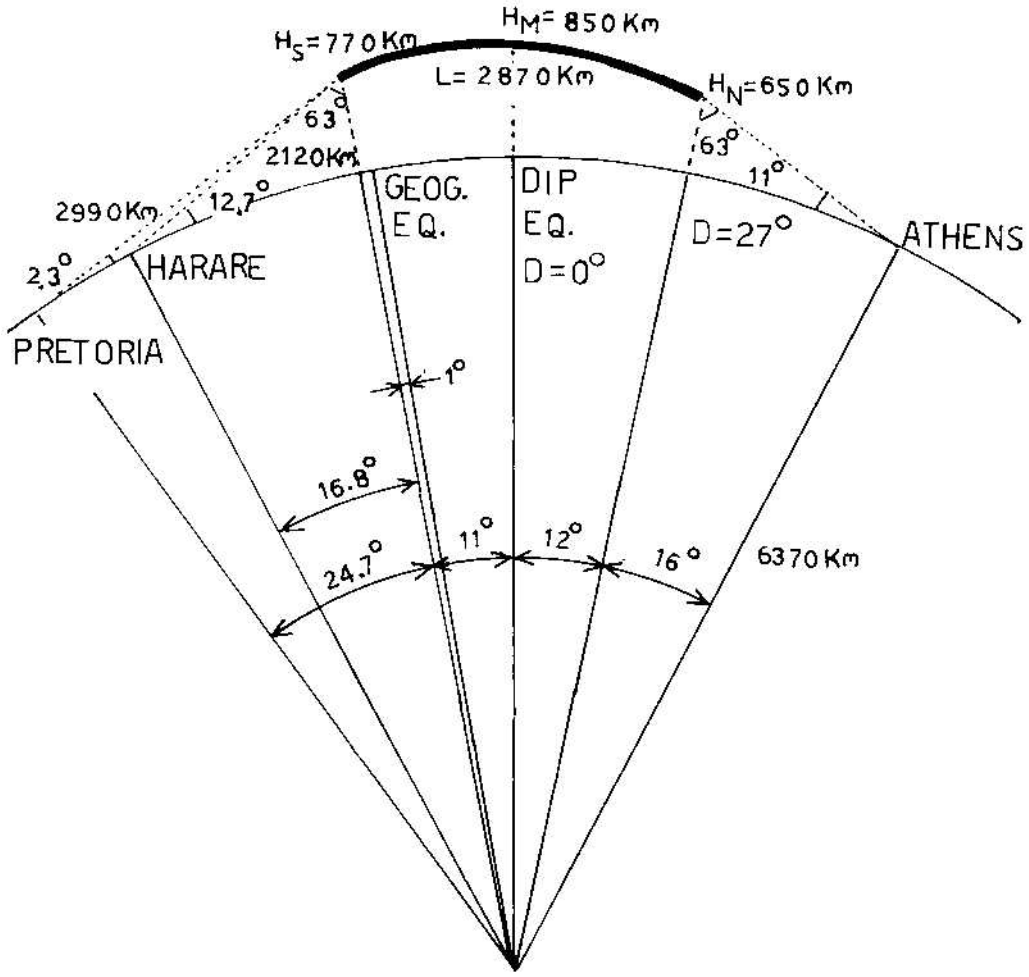

Fig. 2 Evening type Transequatorial propagation circuit geometry.

the actual propagation geometry is illustrated where the great circle passing through Pretoria and Athens is shown. On the same circle approximately the position of Harare is also shown. The intersection point between this specific great circle and the magnetic (dip) equator has a north latitude $+10^{o}$ while the maximum density of the equatorial anomalies is at 24^{o} north and 3^{o} south latitudes respectively. Based on observations during the peak of the 21st solar cycle the ionospheric ducts seems to be extending at least between these latitudes[8] with a maximum height above the magnetic dip equator. The waveguide axis follows approximately the magnetic field of lines. Furthermore for the specific circuit geometries the great circle is almost perpendicular to the magnetic dip equator (80^{o}) and therefore in eq. (27) the angle α is taken almost equal to zero (see fig. 1c).

In order to compare the measured data with the numerical results obtained by using eqs. (27), (28) and the elevation angle at the reception point, a simple computer program has been written. The ionospheric guide characteristics and compiled from the measured values given in ref. 8 and are taken to be a=25 km, $N(o) = 10^{5}cm^{-3}$. The values of G_tG_r are known from the working condition of the stations where the transmission line and antenna pattern losses are included. The waveguide length on each hemisphere and the common axis height h_o above the magnetic dip equator are taken to be unknown.

Measured data is available at 28, 50, 144 and 432 MHz frequencies[2,13]. By running the computer program successively and comparing with the experimental data at 144 MHz for the overall attenuation (average value), incoming elevation angles and total propagation delay, the values of L and h_o giving the best fit are determined. Through this procedure the value of n"(o) is also determined. These values are:

$$L = 2870 \text{ km}, \quad h_o = 850 \text{ km}, \quad n"(o) = 3\cdot10^{-7} \tag{29}$$

and from the geometry of the problem $\vartheta_i \cong \vartheta_s \cong 0.2^{o}$.

It is interesting to compare the predicted overall attenuation at other frequencies (28, 50 and 432 MHz) with the measured data. Employing the values given in (29) the overall attenuation is computed at the 28, 50 and 432 MHz frequencies. In table I the comparison of measured and theoretical attenuation is given in dB units. A reasonable agreement is observed at 50 and 28 MHz on both E-TEP circuits. Note that the measurement accuracy was ±3 dB. These results are obtained by taking n"(o) to be independent of frequency. Initially it was thought reasonable to assume Rayleigh scatterers inside the duct. Then $k_on"(o)$ should vary as f^4 (where f is the frequency) since $k_on"(o)$ is proportional to the total scattering cross section Q. However, computations indicated that n"(o) is independent of frequency and therefore Q is proportional to f. According to this observation it is suggested that the inhomogeneities inside the duct are tenious large size scaterrers.

For the 144 MHz the minimum attenuation when $\vartheta_i=\vartheta_s=0$ is also quoted. Notice that the measured minimum attenuation 196 dB corresponds to an average value while the predicted 147 dB is the absolute minimum. At 432 MHz measurement of attenuation was possible only on the Harare-Athens circuit. In this case because of the very high losses only signals under very favorable conditions (with $\vartheta_i=\vartheta_s=0$) can be measured. Therefore it is reasonable to compare the minimum attenuation rather than average values.

Indeed a rough agreement is observed at 432 MHz Harare-Athens circuit.

In table I comparisons are also given for the total time delay and the elevation angle ψ (only at 144 MHz). In general the agreement is good. The smaller propagation delays observed at lower frequencies are attributed to other ionospheric propagation modes such as double refraction from the crests (^2F) or the conventional $2F_2$ propagation at 28 MHz.

4. CONCLUSIONS

An analysis has been presented for the Evening type Transquatorial Propagation by taking into account the ducts observed in equatorial ionosphere.The overall attenuation between two points located at opposite hemispheres has been computed. The closed form of the obtained results permits easy interpretation of the predicted overall attenuation. Comparison of the measured attenuation at 28, 50, 144 and 432 MHz frequencies with the theoretically predicted values shows a reasonable good agreement.

TABLE I. Comparison of predicted and measured parameter values.

TOTAL MEAN ATTENUATION (db)					
Circuit	Pretoria - Athens			Harare - Athens	
Frequency (MHz)	Theory	Measurement		Theory	Measurement
432	368(187 min)			384 (184 min)	234 (222 min)
144	208(147 min)	208 (196 min)		211	211 (199 min)
50	160	165		158	157
28	155	155		154	147
TIME DELAY (ms)					
		Range	Average		
144	26.10	25.6-26.5	26.0	23.2	-
50	26.12	24.8-26.4	25.2	-	-
28	26.15	24.4-27.2	24.6	-	-
ELEVATION ANGLE IN ATHENS (^{o}) (fig. 1a)					
144	11	$9 \leq \psi < 20$		11	$9 < \psi < 20$

References

1. Nielson, D.L., "A review of VHF Transequatorial propagation", AGARD CP, No. 37, pp. 45.1-45.18, 1968.
2. Cracknell, R.G., Anderson, F. and Fimerelis, C., "The Euro-Asia to Africa VHF Transequatorial circuit during solar cycle 21", QST, Vol. 65(11), pp. 31-36 and Vol. 65(12) pp. 23-27, 1981.
3. Villard, O.G., Skin, S., Yeh, K.C., "Studies of transequatorial io-

nospheric propagation by the scatter sounding method", Jour. of Geophy. Res., Vol. 62, pp. 399-412, 1957.
4. Bowen, E.D., Fay, W.J., Heritage, J.L., "VHF characteristics of the transequatorial ionosphere", Jour. of Geophy. Res., Vol. 73, pp. 2469-2476, 1968.
5. Nielson, D.L., "Long-range VHF propagation across the geomagnetic equator", Report Stanford Res. Inst. (1969).
6. Heron, M.L., McNamara, L.F., "Transequatorial VHF propagation through equatorial plasma bubbles", Radio Science, Vol. 14(5), pp. 897-910, 1979.
7. Winkler, G., "Radio wave guidance at VHF through equatorial plasma bubbles", Jour. Atm. Terrest. Physics, Vol. 43, pp. 307-315, 1981.
8. Tsunoda, R., "Magnetic field-aligned characteristics of plasma bubbles in the night-time equatorial ionosphere", Jour. Atm., Terrest. Phys., vol. 42, pp. 743-752, 1980.
9. Davies, K., "Ionospheric Radio Propagation", Dover Publ., Ch.3, 1966.
10. Unger, H.G., "Planar Optical Waveguides and Fibers", Clarendon Press, Oxford, Ch. 4, 1977.
11. Lebedev, N.N., "Special functions and their applications", Dover Pub., Chapter 4 and 6, 1972.
12. Jones, D.S., "Theory of Electromagnetism", Pergamon Press, Sec. 9.20, 1964.
13. Fimerelis, C., Uzunoglu, N.K., "Experimental results for the 144 MHz Transequatorial Propagation in the Euro-African Sector". IEE Third Int. Conf. Proc. on Antennas and Propagation - ICAP 83, Vol. 1, pp. 325-328, 1983.

APPENDIX

Computation of the series $S(\varphi_s, x_i, x_s)$

In order to compute the series given in eq. (24) the mode propagation constants β_{mn} defined in eq. (9) are approximated as follows

$$\beta_{mn} = k_o n(o)\left(1-\frac{\sqrt{2\Delta}}{k_o n(o) Q}(2n+m+1)\right) \qquad (A.1)$$

which is valid when the second term inside the parenthesis is very smaller than 1. Furthermore use is made of the identity[11]:

$$\sum_{n=0}^{\infty} \frac{n!}{(m+n)!} L_n^{(m)}(\xi) L_n^{(m)}(\eta) t^n = \frac{1}{1-t} e^{-\frac{(\xi+\eta)t}{1-t}} (\xi\eta t)^{-\frac{m}{2}} \cdot I_m\left(\frac{2\sqrt{\xi\eta t}}{1-t}\right) \qquad (A.2)$$

where $I_m(x)$ is the modified Bessel function. Introducing into eq. (A.2) the values

$$t = e^{-j\frac{2\sqrt{2\Delta L}}{a}}, \quad \xi = x_i, \quad \eta = x_s$$

and since

$$I_\nu(q) = j^{-\nu} J_\nu(jq)$$

the series in eq. (24) can be rewritten as follows,

$$S(\varphi_s, x_i, x_s) = \frac{j}{2} e^{-jk_o n(o)L} \frac{\exp\left(-j \frac{(x_i + x_s) e^{j\frac{\sqrt{2\Delta}}{a}L}}{2\sin(\frac{\sqrt{2\Delta}L}{a})}\right)}{\sin(\frac{\sqrt{2\Delta}L}{a})} \cdot$$

$$\cdot \sum_{m=-\infty}^{+\infty} j^{-m} \varepsilon_m \cos(m\varphi_s) J_m\left(\frac{(x_i x_s)^{1/2} e^{j\frac{\sqrt{2\Delta}}{a}L}}{\sin(\frac{\sqrt{2\Delta}L}{a})}\right) \qquad (A.3)$$

Observing that the summation of the series in eq. (A.3) can be determined by using eq. (17) after some straightforward algebraic operations the results given in eq. (25) is obtained.

Send requests for reprints to Nikolaos K. Uzunoglu.